THE EUROPEAN
PHYSICAL JOURNAL C

Distinguish the $f(T)$ model from ΛCDM model with Gravitational Wave observations

Yi Zhang[1,a], **Hongsheng Zhang**[2]

[1] College of Science, Chongqing University of Posts and Telecommunications, Chongqing 400065, China
[2] School of Physics and Technology, University of Jinan, West Road of Nan Xinzhuang 336, Jinan, Shandong 250022, China

Abstract Separately, neither electromagnetic (EM) observations nor gravitational wave (GW) observations can distinguish between the $f(T)$ model and the ΛCDM model effectively. To break this degeneration, we simulate the GW measurement based on the coming observation facilities, explicitly the Einstein Telescope. We make cross-validations between the simulated GW data and factual EM data, including the Pantheon, H(z), BAO and CMBR data, and the results show that they are consistent with each other. Anyway, the EM data itself have the H_0 tension problem which plays critical role in the distinguishable problem as we will see. Our results show that the GW+BAO+CMBR data could distinguish the $f(T)$ theory from the ΛCDM model in 2σ regime.

1 Introduction

The direct detection of gravitational wave (GW) confirms a major prediction of Einstein's General Relativity (GR) and initiates the era of gravitational wave physics [1–9]. Anyway, not only General Relativity (GR) which based on the symmetric metric with Levi-Civita connection could produce GW events, but also the Teleparallel Gravity with Weitaenböck connection [10–13] could produce observable GW events. Until now, 56 GW events have been discovered. In the coming decade, ground-based (e.g.Einstein Telescope (ET) [14,15] and space-based GW (e.g.Taiji [16], Tianqin [17], and LISA [18]) experiments are predicted to discover more GW sources and provide a new and powerful tool to probe the fundamental properties of gravities.

The most accurate observation on late acceleration, Planck data, favors ΛCDM model in GR [19,20]. As an extension of Teleparallel Gravity, the $f(T)$ theory could provide the late acceleration for our universe as well. The EM data can not distinguish the $f(T)$ model from the ΛCDM model

effectively [21–39][1] which denotes the degeneration between Teleparallel Gravity and General Relativity. Furthermore, the Hubble constant H_0 tension between the early EM measurements (e.g. BAO and CMBR) and late EM measurement (e.g, Pantheon and H(z)), which is the most significant, long-lasting and widely persisting tension, is inherited in modified gravity. Specifically, the typical cited prediction from Planck in a flat ΛCDM model for the Hubble constant is $H_0 = 67.27 \pm 0.60$ km/s/Mpc at 68% confidence level (CL) for Planck 2018 [40], while that from the SH0ES Team is $H_0 = 73.2 \pm 1.3$ km/s/Mpc [41] which yields a 4.14σ tension (see e.g. [42] for a review and references therein for various models to solve the H_0 tension proposed so far).

For GW signals, besides the "+" and "×" polarization patterns, the simplest $f(T)$ gravity in four dimensional spacetime provides one extra degrees of freedom, namely a massive vector field. Such an extra degree of tensor perturbation in $f(T)$ Teleparallel Gravity does not propagate because of its Yukawa-like potential. Then, the effective degree of tensor perturbation in $f(T)$ model could be regarded as the same as GR in the Post-Minkowskian limit [43–45]. The literature [33] constrains the $f(T)$ model by using the GW phase effect based on the TaylorF2 GW waveform. It shows that detection sensitivity within ET can improve up two orders of magnitude of the current bound on the $f(T)$ gravity. The TylorF2 form is based on post-Newtonian (PN) method which is related to metric gravity, and uses the stationary phase approximation which assumes slowly varying amplitude and phase. Then, it is necessary to consider the effect of the GW amplitude which is proportional to the luminosity distance [46,47]. The GW sources are distance indicators which is called dark siren as shown in Refs. [48,49]. Furthermore, the propagation of gravitational wave is different in modified gravity and General Relativity [50–54].

---

[1] Reference [39] solves the H_0 tension problem in the frame of effective field theory including torsion which is different from our $f(T)$ models.

Numerical simulations present valuable approach to forecast results of surveys and targeted observations that will be performed with next generation instrument like Einstein Telescope [55–57]. The Einstein Telescope will detect thousands of NSB (Neutron Star Binary) and BHB (Black Hole Binary) mergers to probe the cosmic expansion at high redshifts. In view that only the EM data cannot distinguish the $f(T)$ model from the ΛCDM model effectively, we will simulate the GW data from Einstein Telescope design and the $f(T)$ model parameters. And we try to search the H_0 tension and distinguishable problem in $f(T)$ theory by using the GW data.

The outline of the paper is as follows. In Sect. 2, we introduce the Teleparallel Gravity and two explicit $f(T)$ models (f_pCDM and f_eCDM models). In Sect. 3, we display the differences between EM and GW data. In Sect. 4, we introduce our EM data firstly, and then our simulated GW data. After checking consistence, we combine the GW data and the EM data to constrain the $f(T)$ models separately. In Sect. 5, we discuss the constraining results. At last, in Sect. 6, we concisely summarize this paper.

2 A brief review of $f(T)$ theory

In $f(T)$ cosmology, the action reads,

$$
\begin{aligned}
S &= \int d^4x \sqrt{-g}(f(T) + \Omega_{m0}(1+a)^3) \\
&= \int d^4x \sqrt{-g}(T + F(T) + \Omega_{m0}(1+a)^3),
\end{aligned} \tag{1}
$$

where $\sqrt{-g}$ is the determination of co-tetrad e^A_μ in $f(T)$ model, T is the torsion scalar playing the role of R in GR, Ω_{m0} stand for the present matter energy density, the index "0" denotes the present value, the $F(T)$ term plays the role of acceleration. Here, we neglect the effects of radiation for the evolution of the universe. And, we assume the background manifold to be a spatially flat Friedmann–Robert–Walker (FRW) universe, then the torsion scalar reads $T = -6H^2$ where H is the Hubble parameter. Routinely, one obtains effective energy density ρ_T and effective pressure p_T for the FRW universe,

$$
\rho_T = \frac{1}{16\pi G}(-12H^2 f_T - f + 6H^2), \tag{2}
$$

$$
p_T = \frac{f - T f_T + 2T^2 f_{TT}}{16\pi G(1 + f_T + 2T f_{TT})}, \tag{3}
$$

where $f_T = df/dT$, $f_{TT} = d^2f/dT^2$. For convenience, we define a dimensionless parameter related to cosmological model,

$$
E^2(z) = \frac{H^2}{H_0^2} = \Omega_{m0}(1+z)^3 + (1 - \Omega_{m0})\frac{f - 2T f_T}{T_0 \Omega_{T0}}, \tag{4}
$$

where $\Omega_{T0} = 8\pi G\rho_{T0}/(3H_0^2)$. And, the effective equation of state (EoS) parameter reads

$$
w_{eff} = \frac{p_T}{\rho_T} = -\frac{f/T - f_T + 2T f_{TT}}{[1 + f_T + 2T f_{TT}][f/T - 2f_T]}. \tag{5}
$$

Once $F_T = constant$, then $w_{eff} = -1$, the model comes back to the ΛCDM model. In the following text, we explore one of the most interesting and tractable $f(T)$ models with one extra parameter.

2.1 The power-law form: f_pCDM model

In the literatures, the power-law $f(T)$ model [10] (hereafter f_pCDM model) is an interesting and notable model,

$$
F(T) = \alpha(-T)^b, \tag{6}
$$

where $\alpha = (6H_0^2)^{1-b}(1 - \Omega_{m0})/(2b - 1)$. Essentially the distortion parameter b is the solo new freedom which quantifies deviation from the ΛCDM model. When $b = 0$, this model degenerates to the ΛCDM model.

2.2 The square-root exponential form: f_eCDM model

Then, we introduce the square-root exponential model [11] (henceafter f_eCDM model)

$$
F(T) = \alpha T_0(1 - e^{-p\sqrt{T/T_0}}), \tag{7}
$$

where $\alpha = (1 - \Omega_{m0})(1 - (1 + p)e^{-p})$ and p is a model parameter. A similar model is proposed in literature, in which $f(T) = \alpha T_0(1 - e^{-pT/T_0})$ [30]. For convenience, we set $b = 1/p$. Anyway, $b \to +0$ corresponds to $p \to +\infty$, while $b \to -0$ corresponds to $p \to -\infty$. Then, for us, getting across $b = 0$ means crossing the singularity p. Therefore, in the numerical processes, for convenience, we set the prior $b > 0$ which is favored by Ref. [33]. When $b < 0$, $e^{-p\sqrt{T/T_0}} > 1$ grows exponentially. In numerical calculation, since it is difficult to cross $b = 0$ we just set the prior that $b > 0$.

2.3 A short discussion

In both $f(T)$ models, an additional parameter b appears. When $b = 0$, the $f(T)$ model comes back to ΛCDM model. And $b \neq 0$ in $f(T)$ model indicates an essential deviation from ΛCDM model.

3 The luminosity distance in EM data and GW data

The gravitational wave (GW) standard sirens offer a new independent way to probe the cosmic expansion. From the GW signal, we can measure the luminosity distance d_L^{GW} directly, without invoking the cosmic distance ladder, since the standard sirens are self-calibrating. The gravitational waves from compact systems are viewed as standard sirens to probe the evolution of the universe [48,49]. We can extract luminosity distance from the GW amplitude

$$h_A = \frac{4}{d_L^{GW}} \left(\frac{GM_c}{c^2} \right)^{5/3} \left(\frac{\pi f_{GW}}{c} \right)^{2/3}, \tag{8}$$

where h_A is the GW amplitude, "A" could be "$+$" or "$\times$", d_L^{GW} is the luminosity for gravitational wave, M_c is the chirp mass, and f_{GW} is the GW frequency. Here we ignore the lower index of "A" because the "$+$" or "$\times$" polarization pattern of GW shares the same luminosity form. From Eq.(8), one sees the significant property of GWs, that is, the amplitude of GWs is inversely proportional to its luminosity distance. If the EM counterpart of the GW event is observed, a redshift measurement of the source enables us to constrain the cosmic expansion history. For the $f(T)$ theory, the evolution equation of GW in Fourier form is [43–45],

$$\ddot{h}_k + 3H(1 - \beta_T)\dot{h}_k + \frac{k^2}{a^2} h_k = 0, \tag{9}$$

where the extra friction term reads,

$$\beta_T = -\frac{\dot{f}_T}{3Hf_T} = -\frac{2\dot{H}}{3H^2} \frac{Tf_{TT}}{f_T}. \tag{10}$$

When $\beta_T = 0$, it reduces to the ΛCDM Model in GR gravity. When $f_{TT} = 0$, it means $F(T) = c_1 T + c_2$ where c_1 and c_2 are constants, as the c_1 will be normalized by the T, so $F(T) = constant$, the model comes back to the ΛCDM model. The extra friction term $(3H\beta_T \dot{h}_{ij})$ affects the amplitude of h_{ij}. If $\beta_T > 0$, the damping will be slower. If $\beta_T < 0$, the damping will be more remarkable. Then, if the cosmic evolution is deviated from ΛCDM model, the constraint result of EM data should reveal a non-zero β_T as well.

To simplify the propagation equation of of h_A in $f(T)$ theory, we define a new scale factor $\tilde{a}$ as $\tilde{a}'/\tilde{a} = \mathcal{H}[1 - \beta_T]$, where $\mathcal{H} = a'/a$ and the prime ("'") is respect to the comoving time. And, after defining a new parameter $\chi_k = h_k/\tilde{a}$, the propagation equation of of h_A becomes,

$$\chi_k'' + \left(k^2 - \frac{\tilde{a}''}{\tilde{a}} \right) = 0. \tag{11}$$

When the gravitational wave propagates across cosmological distance, χ_k decreases as $1/\tilde{a}$ rather than $1/a$. In small scale, the term $\tilde{a}''/\tilde{a}$ is negelectable. Then, this effect is best to test in cosmological scale.

As shown in Refs. [50,53], the relation between the EM luminosity distance and GW luminosity distance is

$$d_L^{GW}(z) = \frac{a(z)}{\tilde{a}(z)} d_L^{EM} = d_L^{EM} exp\left(-\int_0^z \frac{dz'}{1+z'} \beta_T(z') \right), \tag{12}$$

where $d_L^{EM} = (1+z)/H_0 \int_0^z d\tilde{z}/E(\tilde{z})$. This equation shows that the extra friction term $(3H\beta_T \dot{h}_{ij})$ makes the EM luminosity data are different from that of GW. Meanwhile, the difficulty of test of luminosity of SN Ia roots in distance, the test of luminosity of GW is redshift. The two observational difficulties are complementary, which can be solved in the meantime by a combined constraint using EM and GW data. The joint EM and GW data are predicted to yield a non-zero β_T and break the parameter degeneration.[2]

4 The data

First, we constrain cosmological models by using realistic EM data and simulated GW data. The EM data contain the Pantheon, H(z), BAO and CMBR data which are widely used in explorations of cosmology. We follow the simulation in Ref. [57] to explore the cosmological constraints on $f(T)$ or General Relativity by simulated data based on Einstein Telescope and the $f(T)$ model. If the simulated GW data are consistent with the EM data, it is reasonable to combine them to constrain cosmologies.

4.1 The EM data

Here, we briefly introduce the Pantheon, H(z), BAO and CMBR data.

The Pantheon sample of 1048 supernovae Ia (SNe Ia), whose redshift range is $0.01 < z < 2.3$, combines the subset of 276 new Pan-STARRS1 (PS1), SNe Ia with useful distance estimates of SNe Ia from SNLS, SDSS, low-z and Hubble space telescope (HST) samples [58] .

In the H(z) measurements, 41 data [59–73] are considered which could be obtained via two ways. One is to calculate the differential ages of passively evolving galaxies, usually called cosmic chronometer. The other is based on the detection of radiation BAO features.

The property of baryon acoustic oscillation (BAO) in the clustering of matter in the universe serves as a robust standard ruler and hence can be used to map the expansion history of the universe. For the BAO data, the ratios of distances and

---

[2] The two sets of data (EM and GW) both indicate $\beta_T \neq 0$ as shown in Table 1, which denotes an acceleration expansion as well.

Table 1 Best fitted values with 1σ and 2σ standard errors for the GW, EW and GW + EM (combined) data for the f_eCDM and f_pCDM models.

f_pCDM	Ω_{m0}	H_0 (km/s/Mpc)	b	β_T	w_{eff}	
GW	$0.263^{+0.048+0.068}_{-0.021-0.089}$	$68.21^{+1.32+2.51}_{-1.32-2.61}$	$-0.122^{+0.624+0.868}_{-0.361-1.023}$	$-0.018^{+0.131+0.152}_{-0.032-0.241}$	$-1.003^{+0.095+0.239}_{-0.146-0.212}$	2.69σ
EM	$0.293^{+0.010+0.020}_{-0.010-0.019}$	$68.41^{+1.23+2.44}_{-1.24-2.41}$	$-0.071^{+0.095+0.171}_{-0.078-0.182}$	$0.012^{+0.017+0.031}_{-0.015-0.033}$	$-1.018^{+0.024+0.047}_{-0.024-0.046}$	2.67σ
GW+Pantheon	$0.197^{+0.047+0.075}_{-0.038-0.083}$	$67.62^{+0.50+0.99}_{-0.50-0.97}$	$0.441^{+0.240+0.349}_{-0.151-0.382}$	$-0.151^{+0.120+0.171}_{-0.061-0.196}$	$-0.861^{+0.070+0.131}_{-0.070-0.131}$	4.01σ
GW+H(z)	$0.262^{+0.020+0.034}_{-0.036-0.014}$	$68.20^{+0.65+1.31}_{-0.65-1.31}$	$0.031^{+0.219+0.395}_{-0.178-0.410}$	$-0.014^{+0.052+0.081}_{-0.031-0.092}$	$-0.987^{+0.050+0.110}_{-0.061-0.110}$	3.46σ
GW+BAO	$0.274^{+0.016+0.031}_{-0.016-0.032}$	$68.40^{+0.63+1.21}_{-0.63-1.21}$	$-0.161^{+0.261+0.412}_{-0.170-0.458}$	$0.022^{+0.038+0.066}_{-0.030-0.070}$	$-1.034^{+0.051+0.099}_{-0.051-0.101}$	3.30σ
GW+CMBR	$0.277^{+0.009+0.019}_{-0.009-0.018}$	$68.61^{+0.57+1.12}_{-0.57-1.12}$	$-0.226^{+0.119+0.203}_{-0.090-0.218}$	$0.036^{+0.014+0.028}_{-0.014-0.029}$	$-1.052^{+0.022+0.043}_{-0.022-0.044}$	3.21σ
GW+Pantheon+H(z)	$0.258^{+0.020+0.035}_{-0.016-0.037}$	$67.77^{+0.50+0.98}_{-0.50-0.98}$	$0.141^{+0.159+0.292}_{-0.141-0.310}$	$-0.037^{+0.047+0.074}_{-0.030-0.083}$	$-0.956^{+0.043+0.097}_{-0.088-0.050}$	3.90σ
GW+Pantheon+BAO	$0.269^{+0.013+0.027}_{-0.013-0.026}$	$67.82^{+0.46+0.90}_{-0.46-0.90}$	$0.042^{+0.110+0.211}_{-0.110-0.279}$	$-0.009^{+0.018+0.050}_{-0.014-0.053}$	$-0.989^{+0.020+0.065}_{-0.072-0.024}$	3.90σ
GW+BAO+CMBR	$0.280^{+0.009+0.017}_{-0.009-0.016}$	$68.51^{+0.57+1.12}_{-0.57-1.12}$	$-0.223^{+0.118+0.221}_{-0.099-0.221}$	$0.035^{+0.016+0.029}_{-0.014-0.032}$	$-1.052^{+0.023+0.048}_{-0.023-0.045}$	3.28σ
GW +EM	$0.286^{+0.007+0.015}_{-0.007-0.014}$	$68.06^{+0.46+0.90}_{-0.46-0.89}$	$-0.117^{+0.086+0.152}_{-0.070-0.160}$	$0.020^{+0.013+0.025}_{-0.013-0.026}$	$-1.030^{+0.019+0.038}_{-0.019-0.038}$	3.73σ

f_eCDM	Ω_{m0}	H_0 (km/s/Mpc)	b	β_T	w_{eff}	Tension
GW	$0.261^{+0.028+0.040}_{-0.015-0.050}$	$67.46^{+0.78+1.33}_{-0.64-1.38}$	$b < 0.404 < 0.708$	$-0.249^{+0.235+0.251}_{+0.046-0.41}$	$-0.869^{+0.034+0.231}_{-0.125-0.154}$	3.88σ
EM	$0.296^{+0.010+0.020}_{-0.010-0.019}$	$67.71^{+1.11+2.10}_{-1.11-2.09}$	$b < 0.162 < 0.251$	$-0.031^{+0.028+0.031}_{-0.013-0.042}$	$-0.959^{+0.014+0.050}_{-0.041-0.042}$	3.21σ
GW+Pantheon	$0.269^{+0.023+0.035}_{-0.014-0.041}$	$67.58^{+0.50+0.97}_{-0.50-0.99}$	$0.261^{+0.154+0.261}_{-0.168-0.261}$	$-0.093^{+0.072+0.090}_{-0.041-0.169}$	$-0.906^{+0.032+0.11}_{-0.091-0.095}$	4.03σ
GW+H(z)	$0.276^{+0.011+0.021}_{-0.011-0.023}$	$67.68^{+0.71+1.11}_{-0.52-1.27}$	$b < 0.282 < 0.432$	$-0.061^{+0.412+0.750}_{-0.411-0.644}$	$-0.923^{+0.022+0.092}_{-0.075-0.077}$	3.84σ
GW+BAO	$0.280^{+0.012+0.023}_{-0.012-0.023}$	$67.67^{+0.60+1.03}_{-0.47-1.08}$	$b < 0.225 < 0.372$	$-0.048^{+0.063+0.121}_{-0.148-0.077}$	$-0.941^{+0.017+0.080}_{-0.059-0.060}$	3.93σ
GW+CMBR	$0.292^{+0.010+0.019}_{-0.010-0.018}$	$67.55^{+0.43+0.82}_{-0.43-0.88}$	$b < 0.145 < 0.233$	$-0.028^{+0.027+0.028}_{-0.009-0.036}$	$-0.963^{+0.012+0.046}_{-0.036-0.037}$	4.13σ
GW+Pantheon+H(z)	$0.278^{+0.011+0.020}_{-0.010-0.023}$	$67.70^{+0.51+0.92}_{-0.46-0.99}$	$0.211^{+0.128+0.168}_{-0.114-0.211}$	$-0.058^{+0.056+0.058}_{-0.024-0.065}$	$-0.929^{+0.041+0.069}_{-0.047-0.071}$	3.96σ
GW+Pantheon+BAO	$0.282^{+0.012+0.021}_{-0.010-0.023}$	$67.64^{+0.45+0.86}_{-0.45-0.92}$	$b < 0.220 < 0.338$	$-0.045^{+0.044+0.045}_{-0.013-0.058}$	$-0.944^{+0.020+0.065}_{-0.056-0.057}$	4.04σ
GW+BAO+CMBR	$0.292^{+0.009+0.018}_{-0.009-0.017}$	$67.54^{+0.42+0.78}_{-0.38-0.84}$	$b < 0.142 < 0.230$	$-0.027^{+0.027+0.027}_{-0.008-0.036}$	$-0.964^{+0.011+0.045}_{-0.035-0.036}$	4.16σ
GW + EM	$0.294^{+0.007+0.015}_{-0.007-0.014}$	$67.84^{+0.36+0.69}_{-0.36-0.74}$	$b < 0.154 < 0.236$	$-0.029^{+0.026+0.029}_{-0.012-0.038}$	$-0.961^{+0.012+0.045}_{-0.038-0.039}$	3.97σ

the so called dilation scale $D_V(z)$ at different redshifts z are taken after [74–76].[3]

The R parameter, which extracts the information in cosmic microwave background (CMB), is defined as

$$R = \sqrt{\Omega_{m0}} \int_0^{z_*} dz'/E(z'), \qquad (13)$$

where $z_* = 1090.43$ denotes the decoupling redshift. We use the first year data of Planck which show $R = 1.7499 \pm 0.0088$ [20].

Roughly speaking, we regard the Pantheon, H(z) data as the late EM measurement, and the BAO and CMBR data as the early one.

4.2 The GW data simulation

The detected GW events are limited, however the upcoming apparatuses for GWs are expected to detect unprecedented amount of GW events. It is an urgent need to simulate the GW data for the upcoming apparatuses to display the

expected improvements in science. We simulated GW data whose $d_L - z$ relation depends on the ET design and the cosmological model parameters Ω_{m0}, H_0 and b. We divide the whole process into two steps. First, we constrain the $f(T)$ models by using the EM data. Then, by using the best fitted value of $f(T)$ models as the fiducial value of the GW simulation, we calculate the GW luminosity distance based on Eq. (12) as the fiducial value. The simulation is parallel the well-known simulation for the case of ΛCDM model [57].

The gravitational waves originate from binary neutron stars or black holes. In the transverse traceless (TT) gauge, the amplitude $h(t)$ can be obtained by detector

$$h(t) = F_+(\theta, \phi, \psi)h_+(t) + F_\times(\theta, \phi, \psi)h_\times(t), \qquad (14)$$

where F_+, $F_\times$ are the antenna pattern functions sensed by the detector, ψ is the polarization angle, and (θ, ϕ) are angles describing the location of the source in the sky relative to the detector. Base on the sensitivity of the Einstein Telescope we study the constraint precision on the cosmological parameters by simulating binary systems of NS-NS and NS-BH that have an accompanying EM signal by using Fisher matrix [57] which is expected 1000 events will be found in the Einstein Telescope in one year. It could be event of NS-BH, or

---

[3] The BAO and $H(z)$ measurements used in this paper are summarized in Table 1 and 2 of Ref. [38].
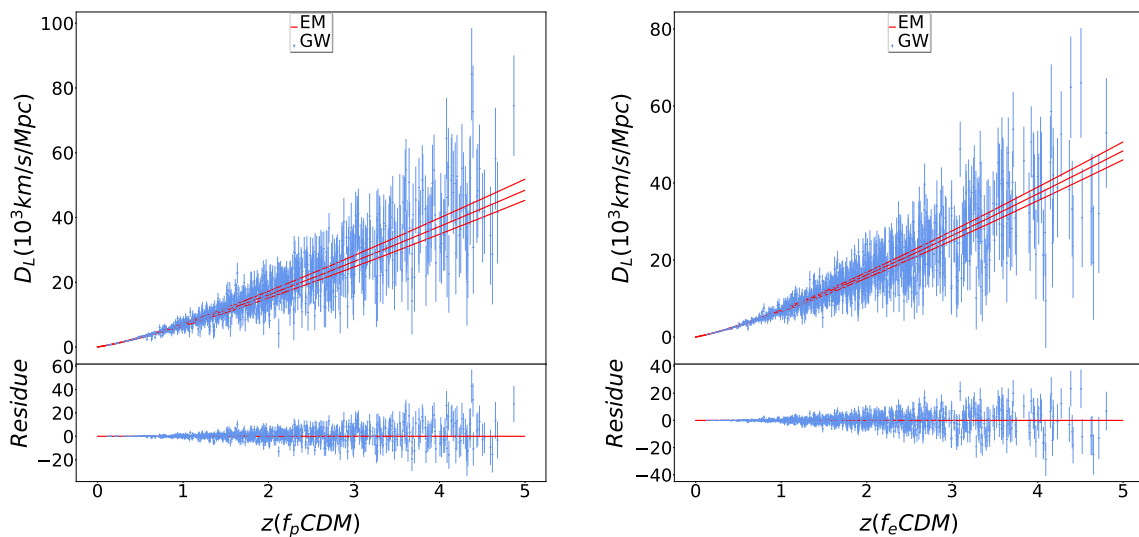
Fig. 1 The data with error-bar are the simulated GW data. The red lines are the best fitted values and the 1σ errors from the EM fitting results. Specifically, the left panel is for the f_pCDM model, while the right panel is for the f_eCDM model

NS-NS. Roughly we assume there are 500 NS-BH events vs 500 NS-NS events. The redshift distribution of the events is followed by Refs. [55–57]. The simulation redshift is chosen as $z < 5$. The performance of a GW detector is characterized by its one-side noise power spectral density (PSD). The PSD of Einstein Telescope is taken to get our error of simulating data as shown in Ref. [56]. Furthermore, the luminosity distance is also affected by an additional error lens due to the weak lensing effects. According to the studies in [55,56], we assume the error is $0.05z$. Thus, the total uncertainty on the measurement of d_L is taken to be

$$\sigma_{d_L} = \sqrt{\sigma_{inst}^2 + \sigma_{lens}^2} = \sqrt{\left(\frac{2d_L}{\rho}\right)^2 + (0.05zd_L)^2}, \quad (15)$$

where ρ is the ratio of signal to noise which is usually chosen as $\rho > 8$. And based on the above discussions , we derive the GW simulated data.

4.3 Data comparison

The Markov Chain Monte Carlo (MCMC) method [77] and the maximum likelihood method are used to constrain the $f(T)$ parameters. Firstly, we constrain the $f(T)$ models by using all the EM data (Pantheon+H(z)+BAO+CMBR). And we use the best fitted values of the results for EM data and ET design to simulate the GW data. We list the simulated GW data and the 1σ fitting results of EM data in Fig. 1.

Comparing the best fitted value of GW data with its fiducial data, we could see the best fitted values of parameter Ω_{m0}, b and H_0 are smaller than the fiducial data. Meanwhile, β_T is smaller the fiducial value and w_{eff} is larger

than the fiducial value. Furthermore, the constraining regions of Ω_{m0}, b, β_T and w_{eff} given by GW constraint are much larger than that of the EM data. While that of GW data lead to a comparative constraint with the EM data for the H_0 parameter. Then, through the fiducial values are changed in the GW data, the best fitted values of all the parameters are still in the 1σ region of the EM constraining results. We calculate the residues by using the 1σ values to subtract the fiducial values. The residues have normal distributions which denote there is no evidence for a systematic difference between GW and EM-based estimated. Then, the simulated GW data are consistent with the EM data. And, the combinations of GW data with the EM data is reasonable.

As the H_0 tension is mainly between the early data and the late data, we consider three ways of combinations. Firstly, we combined GW with the Pantheon, H(z), BAO and CMBR data separately. Then we combined GW to the late measurements(Pantheon + H(z)) and the early measurements (BAO +CMBR) separately. And, the crossing combination (GW+BAO+Pantheon) is added as supplements. At last, we combined them all. To denote the H_0 problem, the data tension [78] is calculated

$$T_1(\theta) = \frac{|\theta(D_1) - \theta(D_2)|}{\sqrt{\sigma_\theta^2(D_1) + \sigma_\theta^2(D_2)}} \quad (16)$$

where θ is chosen as the best fitted values of H_0, the first data set D_1 is separately chosen as the three kinds of data discussed in the above, the second data is set as the SH0Es Teams data ($H_0 = 73.2 \pm 1.3$ km/s/Mpc at 68% confidence level) in this letter.
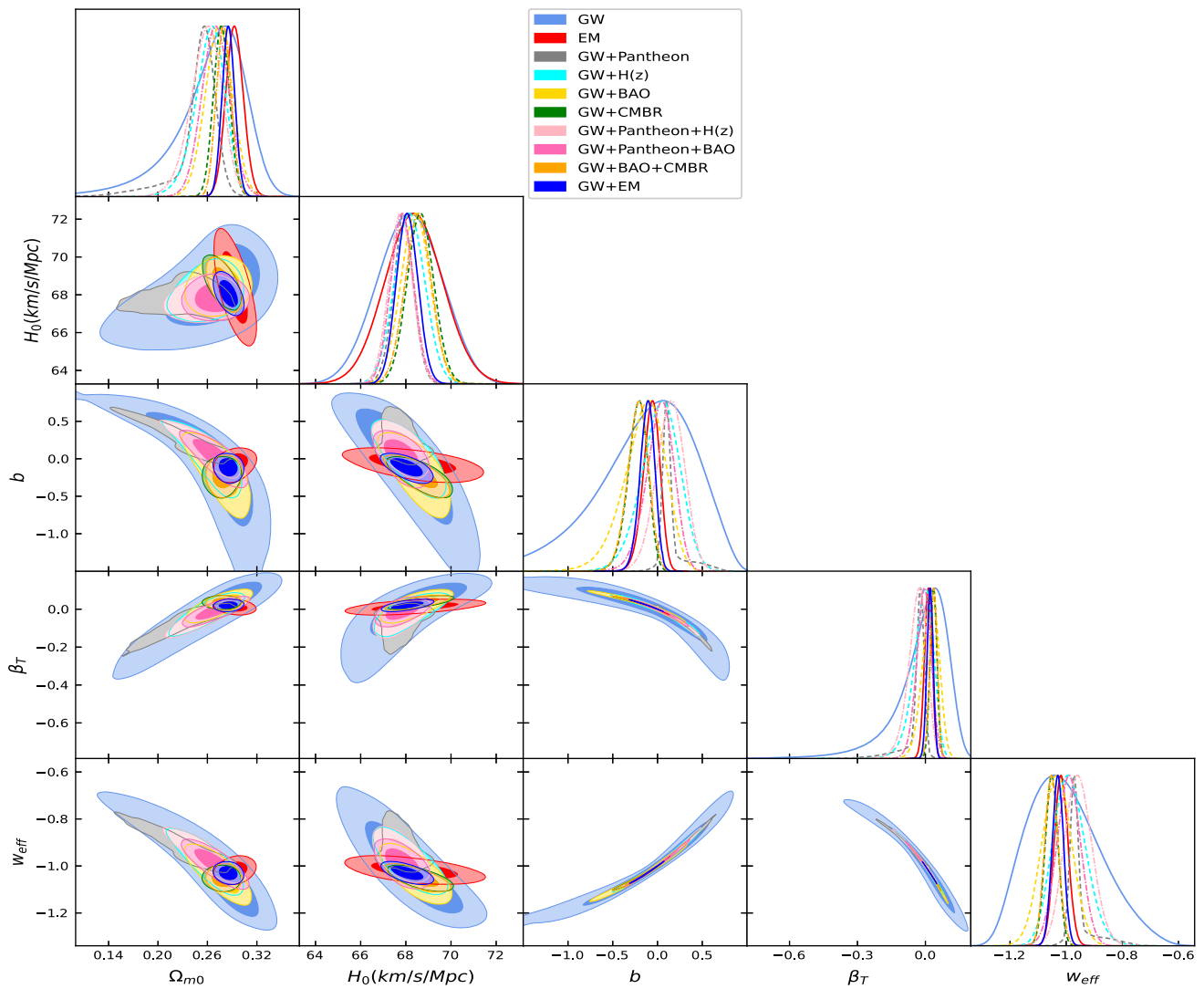
Fig. 2 The probability density functions (pdfs), the 68% (1σ) and 95% (2σ) confidence regions for the parameters (Ω_{m0}, H_0, b, β_T and w_{eff}) in the f_pCDM model respectively
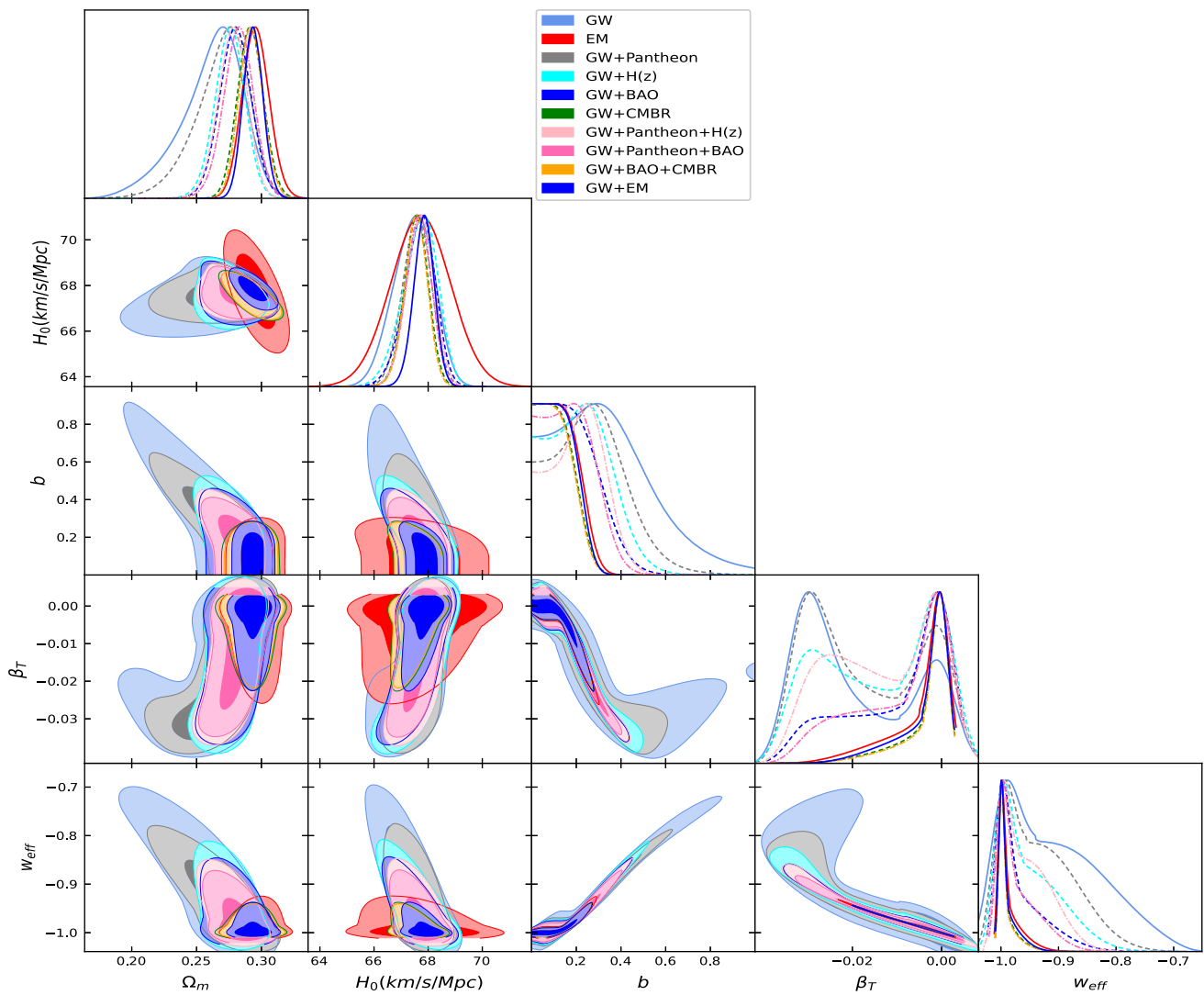
5 Constraining results

In Table 1, we show the constraining results of the constant parameters Ω_{m0}, H_0, and b. Furthermore, we compute the evolving parameters β_T and w_{eff} as well. In Figs. 2 and 3, we present the triangle plots of the parameters which include the probability density function (pdf) and the contours for both $f(T)$ models. In addition, we plot the 1σ evolutions of β_T and w_{eff} in Figs. 4 and 5.[4]

5.1 The f_pCDM model

The contours are closed and smooth and the pdfs are gaussian-distributed in f_pCDM model. Explicitly, either the EM or GW data alone can not distinguish the $f(T)$ model from the ΛCDM model. The constraining tendencies of GW+Pantheon and GW+H(z) data are similar which give out the positive best fitted b and negative best fitted β_T. In the contrast, that of GW+BAO and GW+CMBR data are similar which give the negative best fitted b and positive best fitted β_T. This is caused by the H_0 tension between the early and late EM data, and denotes the parameters β_T and b negatively related.

Because of the H_0 tension, the GW+Pantheon+H(z) and GW+BAO+CMBR both have tight constraining results. And the GW+BAO+CMBR data has the tightest constrain

---

[4] The χ^2 of each model for each data set are equal to the number of degree of freedom, the constraints are reasonable. Especially, the χ^2 of GW data of f_pCDM is smaller than that of f_eCDM. This comparison is trustworthy because the GW data are simulated from different models. Then we do not list the χ^2 values in this letter.

Fig. 3 The probability density functions (pdfs) , the 68% (1σ) and 95% (2σ) confidence regions for the parameters (Ω_{m0}, H_0, b, β_T and w_eff) in the f_eCDM model respectively

while the GW+EM one which includes all the EM data does not. The GW+Pantheon+BAO data has larger contours than the GW +Pantheon+H(z) and GW+BAO+CMBR data which denotes the H_0 tension as well. Obviously, the GW data combined with both the early and late EM data improve the constraint significantly. After the solution of the H_0 tension, the distinguishable problem will be more clear.

The $w_{eff} = 0$ value is not included in 2σ regime for f_pCDM model by the constraining of the GW+BAO+CMBR data. In another saying, the f_pCDM model could be distinguished from ΛCDM in 2σ constraints by adding the GW data. The distinguishable effect is mainly from the β_T parameter which is related to the GW luminosity data and breaks the main degeneration between the parameters.
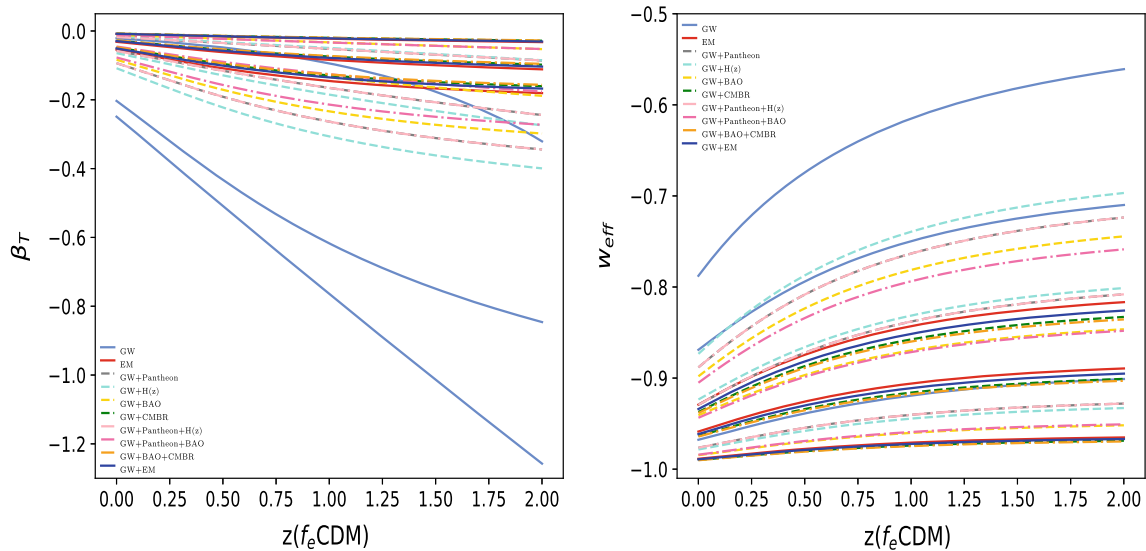
5.2 The f_eCDM model

As shown in Table 1, we obtain a minus β_T and a quintessence-like w_{eff} in f_eCDM model as the setting of the prior $b > 0$. The evolutions of w_{eff} and β_T almost follow ΛCDM model at late time which are quite flat. The contours of β_T have two peaks for f_eCDM model. There is a non-gaussian behavior for b which is caused by the prior $b > 0$. Though the contours related to b are not closed, but the contours related to w_{eff} and β_T are nearly closed.

Generally, the GW+Pantheon data constrains the b parameter more effectively in the f_eCDM model. And, the best fitted value of all the data of the β_T and w_{eff} are close to ΛCDM model. As we set the $b > 0$ prior for f_eCDM model, it does not face to the distinguishable problem.
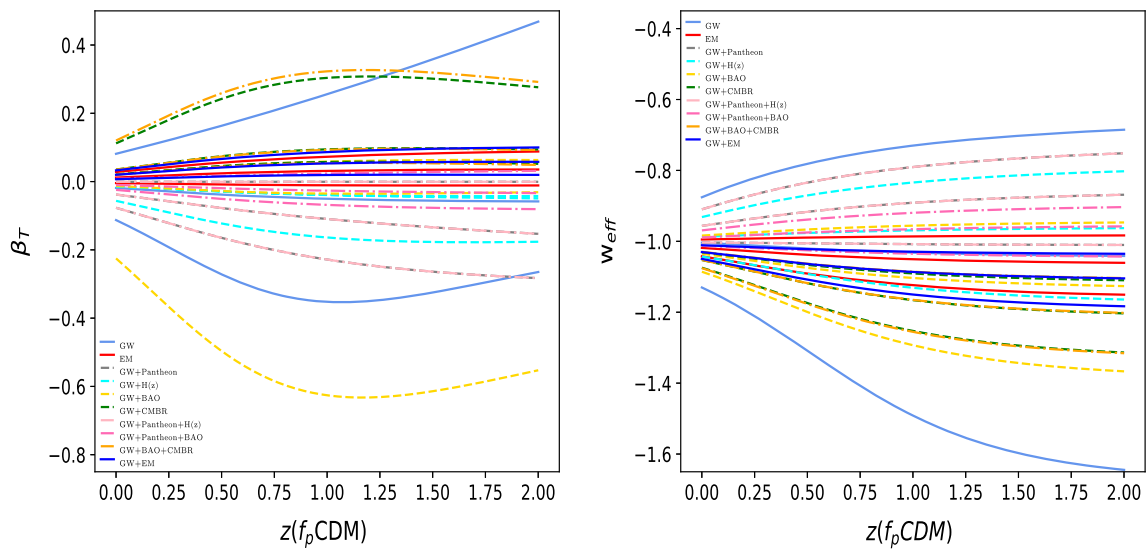
Fig. 4 The evolution of w_{eff} and β_T of the f_pCDM model in 1σ region for the GW, EM and combined data separately

Fig. 5 The evolution of w_{eff} and β_T of the f_eCDM model in 1σ region for the GW, EM and combined data separately

5.3 Short summary

Comparing the constraining results for f_pCDM and f_eCDM models, the 1σ constraining regions of all the GW related data of f_eCDM model are comparable with that of f_pCDM model. The constraining precisions do not sensitive to the prior $b > 0$. And the shape of the $f(T)$ function almost does not affect the constraining precision as well. And considering the tension between our data and the SH0Es data as list in Table 1, the combined data have larger tensions than the GW or EM data, that is mainly because the precision of the data are improved, while the shift of the best-fitted value is slight.

Finally, as shown in Figs. 4 and 5, at high z, the deviations from ΛCDM model become evident. Then more high z data may help to distinguish them.

6 Conclusion

In this paper, we focused on the detection ability of the future GW data to constrain the $f(T)$ models and discussed the related H_0 tension problem. The GW+BAO+CMBR data give the tightest constraints. The GW data are powerful probes to distinguish the modified gravity from the GR, espe-

cially the degenerated ones in view of early EM data. As our computations show, the gravitational wave detections offer a remarkable approach to explore the universe from a new perspective, providing an access to astrophysical processes that are completely ignorant to EM observations.

Data Availability Statement This manuscript has no associated data or the data will not be deposited. [Authors' comment: The data is listed in Table 1.]

References

1. B.P. Abbott et al., [LIGO Scientific and Virgo Collaborations], Phys. Rev. Lett. **116**(6), 061102 (2016). https://doi.org/10.1103/PhysRevLett.116.061102. arXiv:1602.03837

2. B.P. Abbott et al., [LIGO Scientific and Virgo Collaborations], Phys. Rev. Lett. **116**(24), 241103 (2016). https://doi.org/10.1103/PhysRevLett.116.241103. arXiv:1606.04855

3. B.P. Abbott et al., [LIGO Scientific and Virgo Collaborations], Phys. Rev. X **6**(4), 041015 (2016). https://doi.org/10.1103/PhysRevX.6.041015. arXiv:1606.04856

4. B.P. Abbott et al., [LIGO Scientific and Virgo and 1M2H and Dark Energy Camera GW-E and DES and DLT40 and Las Cumbres Observatory and VINROUGE and MASTER Collaborations], Nature **551**(7678), 85 (2017). https://doi.org/10.1038/nature24471. arXiv:1710.05835

5. B.P. Abbott et al., [LIGO Scientific and VIRGO Collaborations], Phys. Rev. Lett. **118**(22), 221101 (2017). https://doi.org/10.1103/PhysRevLett.118.221101. arXiv:1706.01812

6. B.P. Abbott et al., [LIGO Scientific and Virgo Collaborations], Phys. Rev. Lett. **119**(14), 141101 (2017). https://doi.org/10.1103/PhysRevLett.119.141101. arXiv:1709.09660

7. B.P. Abbott et al., [LIGO Scientific and Virgo Collaborations], Astrophys. J. **851**(2), L35 (2017). https://doi.org/10.3847/2041-8213/aa9f0c. arXiv:1711.05578

8. R. Abbott et al., [LIGO Scientific and Virgo], arXiv:2010.14527

9. R. Abbott et al., [LIGO Scientific, KAGRA and VIRGO], Astrophys. J. Lett. **915**(1), L5 (2021). https://doi.org/10.3847/2041-8213/ac082e. arXiv:2106.15163

10. G.R. Bengochea, R. Ferraro, Phys. Rev. D **79**, 124019 (2009). https://doi.org/10.1103/PhysRevD.79.124019. arXiv:0812.1205 [astro-ph]

11. E.V. Linder, Phys. Rev. D **81**, 127301 (2010) [Erratum: Phys. Rev. D **82**, 109902 (2010)]. https://doi.org/10.1103/PhysRevD.81.127301. https://doi.org/10.1103/PhysRevD.82.109902. arXiv:1005.3039 [astro-ph.CO]

12. P. Wu, H.W. Yu, Eur. Phys. J. C **71**, 1552 (2011). https://doi.org/10.1140/epjc/s10052-011-1552-2. arXiv:1008.3669 [gr-qc]

13. Y.F. Cai, S. Capozziello, M. De Laurentis, E.N. Saridakis, Rep. Prog. Phys. **79**(10), 106901 (2016). https://doi.org/10.1088/0034-4885/79/10/106901. arXiv:1511.07586

14. M. Punturo et al., Class. Quantum Gravity **27**, 194002 (2010). https://doi.org/10.1088/0264-9381/27/19/194002

15. B.S. Sathyaprakash, B.F. Schutz, C. Van Den Broeck, Class. Quantum Gravity **27**, 215006 (2010). https://doi.org/10.1088/0264-9381/27/21/215006. arXiv:0906.4151 [astro-ph.CO]

16. W.R. Hu, Y.L. Wu, Natl. Sci. Rev. **4**(5), 685–686 (2017). https://doi.org/10.1093/nsr/nwx116

17. J. Luo et al., Class. Quantum Gravity **33**(3), 035010. https://doi.org/10.1088/0264-9381/33/3/035010. arXiv:1512.02076

18. https://sci.esa.int/web/lisa

19. P.A.R. Ade et al., [Planck Collaboration], Astron. Astrophys. **594**, A13 (2016). https://doi.org/10.1051/0004-6361/201525830. arXiv:1502.01589

20. P. Ade, N. Aghanim, C. Armitage-Caplan, M. Arnaud, M. Ashdown, F. Atrio-Barandela, J. Aumont, C. Bac-cigalupi, A. Banday, R. Barreiro et al., Astron. Astrophys. **571**, A16 (2014)

21. R. Ferraro, AIP Conf. Proc. **1471**, 103 (2012). https://doi.org/10.1063/1.4756821. arXiv:1204.6273 [gr-qc]

22. T. Clifton, P.G. Ferreira, A. Padilla, C. Skordis, Phys. Rep. **513**, 1 (2012). https://doi.org/10.1016/j.physrep.2012.01.001. arXiv:1106.2476 [astro-ph.CO]

23. Y. Zhang, H. Li, Y. Gong, Z.H. Zhu, JCAP **1107**, 015 (2011). https://doi.org/10.1088/1475-7516/2011/07/015. arXiv:1103.0719 [astro-ph.CO]

24. A. Awad, W. El Hanafy, G.G.L. Nashed, E.N. Saridakis, JCAP **1802**(02), 052 (2018). https://doi.org/10.1088/1475-7516/2018/02/052. arXiv:1710.10194

25. K. Bamba, C.Q. Geng, C.C. Lee, arXiv:1008.4036 [astro-ph.CO]

26. A. Paliathanasis, J.D. Barrow, P.G.L. Leach, Phys. Rev. D **94**(2), 023525 (2016). https://doi.org/10.1103/PhysRevD.94.023525. arXiv:1606.00659

27. K. Bamba, C.Q. Geng, C.C. Lee, L.W. Luo, JCAP **1101**, 021 (2011). https://doi.org/10.1088/1475-7516/2011/01/021. arXiv:1011.0508 [astro-ph.CO]

28. S.B. Nassur, M.J.S. Houndjo, I.G. Salako, J. Tossa, arXiv:1601.04538

29. I.G. Salako, M.E. Rodrigues, A.V. Kpadonou, M.J.S. Houndjo, J. Tossa, JCAP **1311**, 060 (2013). https://doi.org/10.1088/1475-7516/2013/11/060. arXiv:1307.0730 [gr-qc]

30. S. Nesseris, S. Basilakos, E.N. Saridakis, L. Perivolaropoulos, Phys. Rev. D **88**, 103010 (2013). https://doi.org/10.1103/PhysRevD.88.103010. arXiv:1308.6142 [astro-ph.CO]

31. R.C. Nunes, S. Pan, E.N. Saridakis, JCAP **1608**(08), 011 (2016). https://doi.org/10.1088/1475-7516/2016/08/011. arXiv:1606.04359 [gr-qc]

32. R.C. Nunes, JCAP **1805**(05), 052. https://doi.org/10.1088/1475-7516/2018/05/052. arXiv:1802.02281 [gr-qc]

33. S. Basilakos, S. Nesseris, F.K. Anagnostopoulos, E.N. Saridakis, JCAP **08**, 008 (2018). https://doi.org/10.1088/1475-7516/2018/08/008. arXiv:1803.09278 [astro-ph.CO]

34. W.S. Zhang, C. Cheng, Q.G. Huang, M. Li, S. Li, X.D. Li, S. Wang, Sci. China Phys. Mech. Astron. **55**, 2244 (2012). https://doi.org/10.1007/s11433-012-4945-9. arXiv:1202.0892 [astro-ph.CO]

35. S. Capozziello, O. Luongo, P. Pincak, A. Ravanpak, Gen. Relativ. Gravit. **50**(5), 53 (2018). https://doi.org/10.1007/s10714-018-2374-4. arXiv:1804.03649

36. R.C. Nunes, S. Pan, E.N. Saridakis, Phys. Rev. D **98**(10), 104055 (2018). https://doi.org/10.1103/PhysRevD.98.104055. arXiv:1810.03942 [gr-qc]

37. R.C. Nunes, M.E.S. Alves, J.C.N. de Araujo, arXiv:1905.03237 [gr-qc]

38. J.Z. Qi, S. Cao, M. Biesiada, X. Zheng, H. Zhu, Eur. Phys. J. C **77**(8), 502 (2017). https://doi.org/10.1140/epjc/s10052-017-5069-1. arXiv:1708.08603 [astro-ph.CO]

39. S.F. Yan, P. Zhang, J.W. Chen, X.Z. Zhang, Y.F. Cai, E.N. Saridakis, Phys. Rev. D **101**(12), 121301 (2020). https://doi.org/10.1103/PhysRevD.101.121301. arXiv:1909.06388 [astro-ph.CO]

40. N. Aghanim et al., Planck, Astron. Astrophys. **641**, A6 (2020). https://doi.org/10.1051/0004-6361/201833910. arXiv:1807.06209 [astro-ph.CO]

41. A.G. Riess, S. Casertano, W. Yuan, J.B. Bowers, L. Macri, J.C. Zinn, D. Scolnic, Astrophys. J. Lett. **908**(1), L6 (2016). https://doi.org/10.3847/2041-8213/abdbaf. arXiv:2012.08534 [astro-ph.CO]

42. E. Di Valentino, O. Mena, S. Pan, L. Visinelli, W. Yang, A. Melchiorri, D.F. Mota, A.G. Riess, J. Silk, arXiv:2103.01183 [astro-ph.CO]

43. K. Bamba, S. Capozziello, M. De Laurentis, S. Nojiri, D. Saez-Gomez, Phys. Lett. B **727**, 194 (2013). https://doi.org/10.1016/j.physletb.2013.10.022. arXiv:1309.2698 [gr-qc]

44. Y.F. Cai, C. Li, E.N. Saridakis, L. Xue, Phys. Rev. D **97**(10), 103513 (2018). https://doi.org/10.1103/PhysRevD.97.103513. arXiv:1801.05827 [gr-qc]

45. H. Abedi, S. Capozziello, Eur. Phys. J. C **78**(6), 474 (2018). https://doi.org/10.1140/epjc/s10052-018-5967-x. arXiv:1712.05933 [gr-qc]

46. T. Baker, E. Bellini, P.G. Ferreira, M. Lagos, J. Noller, I. Sawicki, Phys. Rev. Lett. **119**(25), 251301 (2017). https://doi.org/10.1103/PhysRevLett.119.251301. arXiv:1710.06394 [astro-ph.CO]

47. J.M. Ezquiaga, M. Zumalacrregui, Phys. Rev. Lett. **119**(25), 251304 (2017). https://doi.org/10.1103/PhysRevLett.119.251304. arXiv:1710.05901 [astro-ph.CO]

48. D.E. Holz, S.A. Hughes, Astrophys. J. **629**, 15 (2005). https://doi.org/10.1086/431341. arXiv:astro-ph/0504616

49. B.F. Schutz, Nature **323**, 310 (1986)

50. E. Belgacem, Y. Dirian, S. Foffa, M. Maggiore, Phys. Rev. D **97**(10), 104066 (2018). https://doi.org/10.1103/PhysRevD.97.104066. arXiv:1712.08108 [astro-ph.CO]

51. E. Belgacem et al. [LISA Cosmology Working Group], arXiv:1906.01593 [astro-ph.CO]

52. L. Amendola, I. Sawicki, M. Kunz, I.D. Saltas, JCAP **1808**, 030 (2018). https://doi.org/10.1088/1475-7516/2018/08/030. arXiv:1712.08623 [astro-ph.CO]

53. M. Lagos, M. Fishbach, P. Landry, D.E. Holz, Phys. Rev. D **99**(8), 083504 (2019). https://doi.org/10.1103/PhysRevD.99.083504. arXiv:1901.03321 [astro-ph.CO]

54. G. Calcagni, S. Kuroyanagi, S. Marsat, M. Sakellariadou, N. Tamanini, G. Tasinato, arXiv:1904.00384 [gr-qc]

55. T.G.F. Li, Extracting Physics from Gravitational Waves: Testing the Strong-field Dynamics of General Relativity and Inferring the Large-scale Structure of the Universe, Springer Theses (2015)

56. W. Zhao, C. Van Den Broeck, D. Baskaran, T.G.F. Li, Phys. Rev. D **83**, 023005 (2011). https://doi.org/10.1103/PhysRevD.83.023005. arXiv:1009.0206 [astro-ph.CO]

57. R.B. Cai, T. Yang, Phys. Rev. D **95**(4), 044024 (2017). https://doi.org/10.1103/PhysRevD.95.044024. arXiv:1608.08008 [astro-ph.CO]

58. D.M. Scolnic, D.O. Jones, A. Rest, Y.C. Pan, R. Chornock, R.J. Foley, M.E. Huber, R. Kessler, C. Narayan, A.G. Riess et al., Astro-phys. J. **859**(2), 101 (2018). https://doi.org/10.3847/1538-4357/aab9bb. arXiv:1710.00845 [astro-ph.CO]

59. C. Zhang, H. Zhang, S. Yuan, T.J. Zhang, Y.C. Sun, Res. Astron. Astrophys. **14**(10), 1221 (2014). https://doi.org/10.1088/1674-4527/14/10/002. arXiv:1207.4541 [astro-ph.CO]

60. R. Jimenez, L. Verde, T. Treu, D. Stern, Astrophys. J. **593**, 622 (2003). https://doi.org/10.1086/376595. arXiv:astro-ph/0302560

61. M. Moresco, L. Verde, L. Pozzetti, R. Jimenez, A. Cimatti, JCAP **1207**, 053 (2012). https://doi.org/10.1088/1475-7516/2012/07/053. arXiv:1201.6658 [astro-ph.CO]

62. M. Moresco, Mon. Not. R. Astron. Soc. **450**(1), L16 (2015). https://doi.org/10.1093/mnrasl/slv037. arXiv:1503.01116 [astro-ph.CO]

63. E. Gaztanaga, A. Cabre, L. Hui, Mon. Not. R. Astron. Soc. **399**, 1663 (2009). https://doi.org/10.1111/j.1365-2966.2009.15405.x. arXiv:0807.3551 [astro-ph]

64. J. Simon, L. Verde, R. Jimenez, Phys. Rev. D **71**, 123001 (2005). https://doi.org/10.1103/PhysRevD.71.123001. arXiv:astro-ph/0412269

65. C.H. Chuang, Y. Wang, Mon. Not. R. Astron. Soc. **426**, 226 (2012). https://doi.org/10.1111/j.1365-2966.2012.21565.x. arXiv:1102.2251 [astro-ph.CO]

66. X. Xu, A.J. Cuesta, N. Padmanabhan, D.J. Eisenstein, C.K. McBride, Mon. Not. R. Astron. Soc. **431**, 2834 (2013). https://doi.org/10.1093/mnras/stt379. arXiv:1206.6732 [astro-ph.CO]

67. M. Moresco et al., JCAP **1605**(05), 014 (2016). https://doi.org/10.1088/1475-7516/2016/05/014. arXiv:1601.01701 [astro-ph.CO]

68. C. Blake et al., Mon. Not. R. Astron. Soc. **425**, 405 (2012). https://doi.org/10.1111/j.1365-2966.2012.21473.x. arXiv:1204.3674 [astro-ph.CO]

69. D. Stern, R. Jimenez, L. Verde, M. Kamionkowski, S.A. Stanford, JCAP **1002**, 008 (2010). https://doi.org/10.1088/1475-7516/2010/02/008. arXiv:0907.3149 [astro-ph.CO]

70. L. Samushia et al., Mon. Not. R. Astron. Soc. **429**, 1514 (2013). https://doi.org/10.1093/mnras/sts443. arXiv:1206.5309 [astro-ph.CO]

71. N.G. Busca et al., Astron. Astrophys. **552**, A96 (2013). https://doi.org/10.1051/0004-6361/201220724. arXiv:1211.2616 [astro-ph.CO]

72. A. Font-Ribera et al., [BOSS Collaboration], JCAP **1405**, 027 (2014). https://doi.org/10.1088/1475-7516/2014/05/027. arXiv:1311.1767 [astro-ph.CO]

73. T. Delubac et al., [BOSS Collaboration], Astron. Astrophys. **574**, A59 (2015). https://doi.org/10.1051/0004-6361/201423969. arXiv:1404.1801 [astro-ph.CO]

74. W.J. Percival et al., [SDSS Collaboration], Mon. Not. R. Astron. Soc. **401**, 2148 (2010). https://doi.org/10.1111/j.1365-2966.2009.15812.x. arXiv:0907.1660 [astro-ph.CO]

75. C. Blake et al., Mon. Not. R. Astron. Soc. **418**, 1707 (2011). https://doi.org/10.1111/j.1365-2966.2011.19592.x. arXiv:1108.2635 [astro-ph.CO]

76. F. Beutler et al., Mon. Not. R. Astron. Soc. **416**, 3017 (2011). https://doi.org/10.1111/j.1365-2966.2011.19250.x. arXiv:1106.3366 [astro-ph.CO]

77. A. Lewis, S. Bridle, Phys. Rev. D **66**, 103511 (2002). https://doi.org/10.1103/PhysRevD.66.103511 [astro-ph/0205436]

78. M. Raveri, W. Hu, Phys. Rev. D **99**(4), 043506 (2019). https://doi.org/10.1103/PhysRevD.99.043506. arXiv:1806.04649 [astro-ph.CO]. https://iopscience.iop.org/article/10.3847/2041-8213/ac082e/pdf